

ANGULAR MOMENTUM AND GALAXY FORMATION REVISITED: SCALING RELATIONS FOR DISKS AND BULGES

S. MICHAEL FALL¹ AND AARON J. ROMANOWSKY^{2,3}

¹*Space Telescope Science Institute, 3700 San Martin Drive, Baltimore, MD 21218, USA*

²*Department of Physics & Astronomy, San José State University, One Washington Square, San Jose, CA 95192, USA*

³*University of California Observatories, 1156 High Street, Santa Cruz, CA 95064, USA*

ABSTRACT

We show that the stellar specific angular momentum j_* , mass M_* , and bulge fraction β_* of normal galaxies of all morphological types are consistent with a simple model based on a linear superposition of independent disks and bulges. In this model, disks and bulges follow scaling relations of the form $j_{*d} \propto M_{*d}^\alpha$ and $j_{*b} \propto M_{*b}^\alpha$ with $\alpha = 0.67 \pm 0.07$ but offset from each other by a factor of 8 ± 2 over the mass range $8.9 \leq \log(M_*/M_\odot) \leq 11.8$. Separate fits for disks and bulges alone give $\alpha = 0.58 \pm 0.10$ and $\alpha = 0.83 \pm 0.16$, respectively. This model correctly predicts that galaxies follow a curved 2D surface in the 3D space of $\log j_*$, $\log M_*$, and β_* . We find no statistically significant indication that galaxies with classical and pseudo bulges follow different relations in this space, although some differences are permitted within the observed scatter and the inherent uncertainties in decomposing galaxies into disks and bulges. As a byproduct of this analysis, we show that the j_* – M_* scaling relations for disk-dominated galaxies from several previous studies are in excellent agreement with each other. In addition, we resolve some conflicting claims about the β_* -dependence of the j_* – M_* scaling relations. The results presented here reinforce and extend our earlier suggestion that the distribution of galaxies with different β_* in the j_* – M_* diagram constitutes an objective, physically motivated alternative to subjective classification schemes such as the Hubble sequence.

Keywords: galaxies: elliptical and lenticular — galaxies: evolution — galaxies: fundamental parameters — galaxies: kinematics and dynamics — galaxies: spiral — galaxies: structure

1. INTRODUCTION

Specific angular momentum ($j = J/M$) and mass (M) are two of the most basic properties of galaxies. Together, they largely determine another basic property—characteristic size (such as half-mass radius R_h)—especially for disk-dominated galaxies. Thus, the correlation between j and M constitutes one of the most fundamental scaling relations for galaxies, as important as those between rotation velocity, velocity dispersion, characteristic size, and mass. We have studied the galactic j – M relation from both observational and theoretical perspectives (Fall 1983; Romanowsky & Fall 2012; Fall & Romanowsky 2013, hereafter Papers 0, 1, and 2). The present paper is a continuation of this series. In the following, when relevant, we distinguish between the stellar, baryonic, and halo parts of galaxies with the subscripts \star , bary, and halo, and between their disk and bulge components with the subscripts d and b.

We have found that both disk-dominated galaxies and bulge-dominated galaxies (mainly ellipticals) obey

power-law scaling relations of the form $j_\star \propto M_\star^\alpha$ with essentially the same exponent, $\alpha = 0.6 \pm 0.1$, and normalizations that differ by a factor of ~ 5 . Our results are based on a sample in which most galaxies have classical bulges (genuine spheroids) rather than pseudo bulges (disk-like structures). In a plot of $\log j_\star$ against $\log M_\star$, galaxies of different morphological type and bulge fraction $\beta_\star \equiv M_{\star b}/(M_{\star d} + M_{\star b})$ follow nearly parallel relations, filling the region between the sequences of disk-dominated and bulge-dominated galaxies. Based on this finding, we have proposed that the distribution of galaxies with different β_\star in the j_\star – M_\star diagram constitutes an objective, physically motivated alternative to subjective classification schemes such as the Hubble sequence.

The parallel sequences of galaxies of different bulge fraction in the j_\star – M_\star diagram suggest a picture in which galactic disks and spheroids are essentially independent objects, formed by distinct physical processes. Disks likely formed relatively quiescently by diffuse gas settling within dark-matter halos, while spheroids likely formed

more violently by colliding streams and clumps of cold gas and by merging of smaller galaxies. Disk-dominated galaxies are those in which major mergers played little or no role, while spheroid-dominated galaxies either never acquired a substantial disk or else acquired one and later lost it by stripping or merging. In this picture, most normal galaxies may be regarded, in a first approximation, as a linear superposition of a flat disk and a round spheroid, each of which lies along the corresponding j_\star - M_\star sequence. The primary purpose of this paper is to make a quantitative test of this picture.

The observed j_\star - M_\star scaling relations also link well with galaxy-formation theory. The galactic halos that form by hierarchical clustering in a dark-matter dominated universe (such as Λ CDM) obey the scaling relation $j_{\text{halo}} \propto M_{\text{halo}}^\alpha$ with $\alpha = 2/3$, an exponent remarkably similar to that for the stellar parts of galaxies. The halo scaling relation follows directly from the fact that the spin parameter λ_{halo} and mean internal density $\bar{\rho}_{\text{halo}}$ are independent of M_{halo} . By comparing the j_\star - M_\star and j_{halo} - M_{halo} relations, mediated by an M_\star - M_{halo} relation, we found that galactic disks have a fraction of specific angular momentum relative to their surrounding halos of $f_j \equiv j/j_{\text{halo}} \approx 0.8$, while galactic spheroids have a fraction $f_j \approx 0.15$. The first of these agrees well with the postulated value $f_j \approx 1$ in simple analytical models of galactic disk formation (Fall & Efstathiou 1980; Dalcanton et al. 1997; Mo et al. 1998).

The j - M scaling relations have been the focus of further observational study, both for low-redshift galaxies (Obreschkow & Glazebrook 2014; Cortese et al. 2016; Butler et al. 2017; Chowdhury & Chengalur 2017; Elson 2017; Kurapati et al. 2018; Lapi et al. 2018b; Posti et al. 2018a; Rizzo et al. 2018; Sweet et al. 2018) and for high-redshift galaxies (Burkert et al. 2016; Contini et al. 2016; Harrison et al. 2017; Shi et al. 2017; Swinbank et al. 2017; Tadaki et al. 2017; Alcorn et al. 2018). Several recent studies have examined the relation between galaxy sizes and halo sizes, a corollary of the j - M relation (Kravtsov 2013; Kawamata et al. 2015; Shibuya et al. 2015; Huang et al. 2017; Kawamata et al. 2018; Okamura et al. 2018). The j - M scaling relations have been a benchmark for some recent analytical and semi-analytical models (Stevens et al. 2016; Shi et al. 2017; Lapi et al. 2018a; Posti et al. 2018b; Zoldan et al. 2018). They have also been the targets of many recent hydrodynamical simulations, some with large volume but relatively low resolution (Genel et al. 2015; Pedrosa & Tissera 2015; Teklu et al. 2015; Zavala et al. 2016; DeFelippis et al. 2017; Lagos et al. 2017; Stevens et al. 2017; Lagos et al. 2018; Schulze et al. 2018) and others with small volume (zoom-in) but higher resolution

(Agertz & Kravtsov 2016; Grand et al. 2017; Sokołowska et al. 2017; El-Badry et al. 2018; Obreja et al. 2018).

The studies cited above generally confirm our j_\star - M_\star scaling relations, particularly the exponent $\alpha \approx 0.6$ for disk-dominated galaxies. The exceptions to this near-consensus are the works by Obreschkow & Glazebrook (2014) and Sweet et al. (2018), which found $\alpha \approx 1.0$ for galaxies of the same bulge fraction, including $\beta_\star = 0$. Obreschkow & Glazebrook (2014) interpreted this to mean that the angular momenta of galactic disks are influenced in some way by the prominence of galactic bulges, i.e., that these two components are not independent, in contradiction to the picture discussed above. Complicating this comparison, however, is the fact that most of the galaxies in the Obreschkow & Glazebrook (2014) and Sweet et al. (2018) samples have pseudo bulges rather than classical bulges. Thus, a secondary purpose of this paper is to resolve the apparent discrepancy between their work and ours.

The remainder of this paper is organized as follows. In Section 2, we compare and contrast four determinations of the j_\star - M_\star relation for galaxies of different bulge fraction, revealing some important similarities and differences. In Section 3, we present the corresponding two-dimensional (2D) surfaces defined by these relations in the three-dimensional (3D) space of j_\star , M_\star , and β_\star , and show that they are consistent with our picture of independent disks and spheroids. We summarize our results and discuss their implications in Section 4. We make some detailed comparisons between our estimates of j_\star , M_\star , and β_\star and those of others in the Appendix.

2. 2D RELATIONS BETWEEN j_\star AND M_\star

Before we consider the distribution of galaxies in the 3D space of specific angular momentum j_\star , mass M_\star , and bulge fraction β_\star , it is helpful to review several determinations of the 2D scaling relations between j_\star and M_\star for galaxies in different ranges of β_\star . In particular, we focus on the results from our work (Paper 2), Obreschkow & Glazebrook (2014), Posti et al. (2018a), and Sweet et al. (2018). These four j_\star - M_\star scaling relations are plotted here in Figure 1, with galaxies of different β_\star represented by symbols of different colors and shapes. Evidently, there are some important similarities and differences between them (Section 2.2). In order to understand why they agree in some respects and disagree in others, we briefly review some of the key assumptions and procedures involved in their derivations (Section 2.1). For a more complete description of how these j_\star - M_\star scaling relations were derived, we refer interested readers to the original papers.

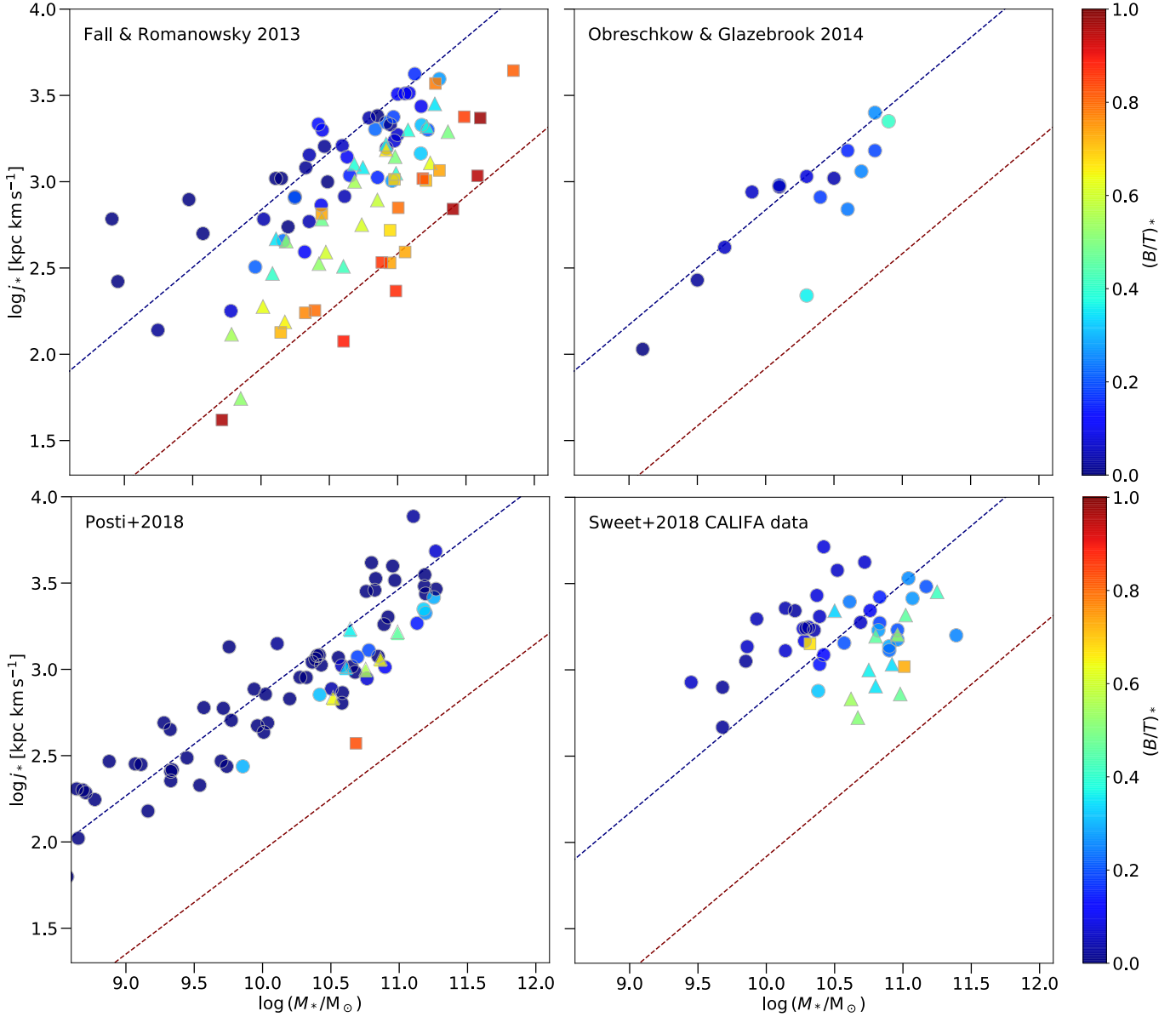


Figure 1. Stellar specific angular momentum j_* plotted against stellar mass M_* for galaxies of different stellar bulge fraction, $\beta_* \equiv (B/T)_*$, from the references indicated in the upper-left corners of the panels. The colors and shapes of the plotted symbols indicate the bulge fractions, with circles for $0 \leq \beta_* < 1/3$, triangles for $1/3 \leq \beta_* < 2/3$, and squares for $2/3 \leq \beta_* \leq 1$. In all four panels, the parallel dashed lines represent the j_* – M_* scaling relations for disks and bulges derived from the 3D fits of Equations (2) and (3) to our dataset as described in Section 3. Note that the scaling relations for disk-dominated galaxies from our work, Obreschkow & Glazebrook (2014), and Posti et al. (2018a) are in excellent agreement with each other, while that from Sweet et al. (2018) is offset from the others. Note also that these samples, with the exception of ours, are largely devoid of bulge-dominated galaxies.

2.1. Samples and Methods

Our j_\star – M_\star relation is based on a sample of 94 galaxies: 57 spirals, 14 lenticulars, and 23 ellipticals.¹ This sample spans a wide range of mass, $8.9 \leq \log(M_\star/M_\odot) \leq 11.8$, and the full range of bulge fraction, $0 \leq \beta_\star \leq 1.0$, with median $\beta_\star = 0.35$. The main selection criterion for this sample was the availability of photometric and kinematic data extending to large radii: $\sim 2R_e$ in all cases and up to $\sim 10R_e$ in some cases (where R_e is the effective or projected half-light radius). The large radial extent of the data has allowed us to obtain convergent estimates of j_\star and M_\star with relatively little extrapolation beyond the outermost measurements (see Section 3 of Paper 1). Most of the surface brightness profiles of the disks and bulges of spiral galaxies come from Kent (1986, 1987, 1988). His method of decomposition matches the 2D images of galaxies with combinations of disks and bulges with pre-specified 3D shapes (flat and round) rather than pre-specified surface brightness profiles (exponential and Sérsic). We estimated the bulge fractions of lenticular and elliptical galaxies from the observed ratios of stellar rotation velocities and velocity dispersions (v_\star/σ_\star), as calibrated by photometric decompositions (see Appendix D of Paper 1).

For spiral galaxies, we estimated the specific angular momentum and mass separately for the disk and bulge components, namely $(j_{\star d}, j_{\star b})$ and $(M_{\star d}, M_{\star b})$. This was necessary because these disks and bulges have distinct mass-to-light ratios, indicated by their colors, and distinct kinematics. For each disk, we derived $j_{\star d}$ directly from the surface brightness profile and the H α or H I rotation curve (or approximations to them), while for each bulge we derived $j_{\star b}$ indirectly from the surface brightness profile and the rotation velocity $v_{\star b}$ estimated from the velocity dispersion $\sigma_{\star b}$ and ellipticity ϵ_b and the mean relation between $v_{\star b}/\sigma_{\star b}$ and ϵ_b for the bulges of similar galaxies. We then combined our estimates of specific angular momentum and mass for each component into the corresponding totals, $j_\star = (j_{\star d}M_{\star d} + j_{\star b}M_{\star b})/M_\star$ and $M_\star = M_{\star d} + M_{\star b}$, for each spiral galaxy. For lenticular and elliptical galaxies, which have disks and bulges of similar mass-to-light ratio, we estimated the total values j_\star and M_\star directly from the overall surface brightness profiles and stellar rotation profiles derived from optical absorption-line spectra and globular cluster and planetary nebula velocities.

In Paper 1, we estimated the stellar masses of both disks and bulges from their K -band ($2.2 \mu\text{m}$) luminosities and an assumed universal mass-to-light ratio, $M_\star/L_K = 1.0$. Subsequently, in Paper 2, we revised our mass estimates for disks and bulges based on their observed $B - V$ colors and the predicted relation between M_\star/L_K and $B - V$ from stellar population models with different star formation histories. These revisions are fairly modest, with typical values $(M_\star/L_K)_d \approx 0.5$ for the disks of late-type spirals, and $(M_\star/L_K)_b \approx 0.8$ for all bulges. The revised mass-to-light ratios do not affect the specific angular momenta of the disk and bulge components derived in Paper 1, but they do affect the total values j_\star , as these are mass-weighted sums of $j_{\star d}$ and $j_{\star b}$. We used, but did not publish, the resulting estimates of j_\star , M_\star , and β_\star in Paper 2; we list them here in Table 1 and plot them in Figure 1.

The Obreschkow & Glazebrook (2014) j_\star – M_\star relation is based on 16 late-type spiral galaxies in the THINGS² survey with *Spitzer* 3.6 μm surface photometry and H I rotation curves from Leroy et al. (2008). This sample spans a moderate range of mass, $9.1 \leq \log(M_\star/M_\odot) \leq 10.9$, but only a narrow range of bulge fraction, $0 \leq \beta_\star \leq 0.3$, with median $\beta_\star = 0.10$. Obreschkow & Glazebrook (2014) decomposed these galaxies by fitting a parametric model with an exponential disk and a Sérsic bulge to the observed surface brightness profiles. The masses of the galaxies were estimated using an empirical conversion between 3.6 μm and K -band luminosities and an assumed universal mass-to-light ratio, $M_\star/L_K = 0.5$, for both disks and bulges. The specific angular momenta were estimated from the H I rotation curves, assuming that the stellar disks and bulges corotate with each other and with the H I. Obreschkow & Glazebrook (2014) derived both the stellar and baryonic j – M scaling relations for this sample (including both stars and cold gas in the latter) and found that they were remarkably similar. For direct comparison with the other j_\star – M_\star relations, we plot only their stellar relation in Figure 1.

The Posti et al. (2018a) j_\star – M_\star relation is based on 92 spiral galaxies, mostly of late type, in the SPARC³ survey with *Spitzer* 3.6 μm surface photometry and H I rotation curves from Lelli et al. (2016). This sample spans an exceptionally large range of mass, $7.0 \leq \log(M_\star/M_\odot) \leq 11.3$, and a narrow range of bulge fraction, with $0 \leq \beta_\star \leq 0.3$ for 90% of the galaxies. Posti et al. (2018a) adopted the decompositions of these galax-

¹ This sample is the same as the one in Paper 2 (despite a misprint there) but differs from the one in Tables 3–5 of Paper 1 because 11 galaxies lack color information and two are peculiar.

² THINGS is an acronym for The HI Nearby Galaxy Survey.

³ SPARC is an acronym for Spitzer Photometry and Accurate Rotation Curves.

ies from Lelli et al. (2016), who fitted a non-parametric model consisting of an unspecified bulge and inner disk and an exponential outer disk to the observed surface brightness profiles. The masses of the disks and bulges were estimated from their 3.6 μm luminosities and the adopted mass-to-light ratios $(M_\star/L_{[3.6]})_{\text{d}} = 0.5$ and $(M_\star/L_{[3.6]})_{\text{b}} = 0.7$, corresponding to $(M_\star/L_K)_{\text{d}} \approx 0.4$ and $(M_\star/L_K)_{\text{b}} \approx 0.6$. Posti et al. (2018a) estimated the specific angular momenta from the H I rotation curves, assuming that the stellar disks and bulges corotate with each other but with a small lag (asymmetric drift) relative to the H I.

The j_\star – M_\star relation published by Sweet et al. (2018) is based on 50 galaxies in the CALIFA⁴ survey, 16 galaxies in the THINGS survey, and 25 galaxies in our sample, with j_\star and M_\star estimated by different methods for each of these subsamples. For galaxies in the THINGS survey and in our sample, the values of j_\star and M_\star were taken directly or adapted from Obreschkow & Glazebrook (2014) and from our Paper 1, respectively. Here, we consider only the CALIFA part of the Sweet et al. (2018) j_\star – M_\star relation, in order to make meaningful comparisons with the other j_\star – M_\star relations derived by different authors from independent samples of galaxies.

The CALIFA part of the Sweet et al. (2018) j_\star – M_\star relation is based on galaxies of all morphological types except diskless ellipticals, with optical surface photometry from Méndez-Abreu et al. (2017) and integral-field spectroscopy from Falcón-Barroso et al. (2017). This sample spans a moderate range of mass, $9.5 \leq \log(M_\star/M_\odot) \leq 11.4$, and a moderate range of bulge fraction, $0 \leq \beta_\star \leq 0.7$, with median $\beta_\star = 0.2$. Sweet et al. (2018) adopted the decompositions of these galaxies from Méndez-Abreu et al. (2017), who fitted a parametric model with an exponential disk (with a possible upward or downward outer bend) and a Sérsic bulge to the observed 2D isophotes. The total masses M_\star , taken from Falcón-Barroso et al. (2017), were estimated from total luminosities in several bands and mass-to-light ratios predicted by stellar population models that matched the observed colors (as described by Walcher et al. 2014). Sweet et al. (2018) estimated the total specific angular momenta j_\star from the projected density and velocity maps derived from the surface photometry and integral-field spectroscopy of stellar absorption lines, assuming that all stars move on coplanar circular orbits (with no velocity dispersion).

⁴ CALIFA is an acronym for Calar Altar Legacy Integral Field Area.

In summary, for spiral galaxies, our study and those of Obreschkow & Glazebrook (2014) and Posti et al. (2018a) adopted similar methods for estimating the disk contributions to j_\star (from H α and H I rotation curves) and M_\star (from near-IR luminosities and similar mass-to-light ratios). However, these studies differed substantially in their treatment of bulges: first, in the methods of disk–bulge decomposition, and second in the assumptions about whether or not disks and bulges have the same rotation velocities. The simplifying assumption that disks and bulges corotate, made by Obreschkow & Glazebrook (2014) and Posti et al. (2018a), leads to acceptably small errors in j_\star for disk-dominated galaxies but not for bulge-dominated galaxies. Since our study aimed to derive the j_\star – M_\star relation over the full range of bulge fractions, we estimated the bulge contributions to j_\star for spiral galaxies indirectly from the velocity dispersion and ellipticity of their bulges, independently of the H α and H I rotation curves of their disks, and the total j_\star for lenticular and elliptical galaxies directly from the stellar rotation profiles.

Based on the tests described in Paper 1, we estimate the following typical errors: $\varepsilon(\log j_\star) \approx 0.15$, $\varepsilon(\log M_\star) \approx 0.10$, and $\varepsilon(\beta_\star) \approx 0.10$ for spiral galaxies and $\varepsilon(\log j_\star) \approx 0.20$, $\varepsilon(\log M_\star) \approx 0.10$, and $\varepsilon(\beta_\star) \approx 0.20$ for lenticular and elliptical galaxies. These are meant to include all sources of uncertainty and thus to represent *total* errors. In particular, they include uncertainties in radial extrapolations of photometric and kinematic data, inclination angles, mass-to-light ratios, and distances. They also include the inevitable deviations of real galaxies from the idealizations required to decompose them into disks and bulges (either pre-specified 3D shapes or surface-brightness profiles) and from the assumptions about bulge rotation. In comparison with these uncertainties, measurement errors are usually negligible. The errors in $\log j_\star$, $\log M_\star$, and β_\star quoted by Obreschkow & Glazebrook (2014), Posti et al. (2018a), and Sweet et al. (2018) are smaller than our estimates because they exclude one or more sources of uncertainty mentioned above and therefore represent *partial* errors. (See Section 2.2 and the Appendix for further discussion of the errors.)

2.2. Comparison of Results

Figure 1 reveals some interesting similarities and differences between the results from these four studies. The first conclusion apparent from Figure 1 is that the j_\star – M_\star relations for disk-dominated galaxies from our Paper 2, Obreschkow & Glazebrook (2014), and Posti et al. (2018a) agree remarkably well with each other. We quantify this impression by fitting a power-law model in

the form

$$\log(j_*/j_0) = \alpha \log(M_*/M_0), \quad (1)$$

with $\log(M_0/M_\odot) = 10.5$, by least-squares minimization in the j_* direction and bootstrap uncertainty analysis, over the mass range $9.5 \leq \log(M_*/M_\odot) \leq 11.5$. Restricting the fits to galaxies with $\beta_* \leq 0.1$, i.e., essentially pure disks (within the uncertainties in β_*), we find $\alpha = 0.58 \pm 0.10$, $\log j_0 = 3.07 \pm 0.03$, and $\sigma(\log j_*) = 0.16$ for our dataset, $\alpha = 0.63 \pm 0.08$, $\log j_0 = 3.16 \pm 0.04$, and $\sigma(\log j_*) = 0.09$ for the Obreschkow & Glazebrook (2014) dataset, and $\alpha = 0.61 \pm 0.06$, $\log j_0 = 3.10 \pm 0.03$, and $\sigma(\log j_*) = 0.19$ for the Posti et al. (2018a) dataset (with j_0 expressed in units of kpc km s^{-1}).

These j_* – M_* relations are virtually identical within the statistical errors, both in exponent ($\alpha \approx 0.6$) and normalization ($\log j_0 \approx 3.1$). The dispersions of individual points about the mean relations in the vertical direction are also similar ($\sigma(\log j_*) \approx 0.1$ – 0.2) and roughly consistent with the corresponding typical error $\varepsilon(\log j_*)$. We make some further comparisons between our dataset and those of Obreschkow & Glazebrook (2014) and Posti et al. (2018a) in the Appendix. In particular, we compare the independent estimates of j_* , M_* , and β_* for the 6–10 galaxies in common between these samples. The mean offsets are small and the dispersions are $\sigma(\log j_*) = 0.11$, $\sigma(\log M_*) = 0.10$, and $\sigma(\beta_*) = 0.09$, again roughly consistent with the corresponding typical errors $\varepsilon(\log j_*)$, $\varepsilon(\log M_*)$, and $\varepsilon(\beta_*)$. These comparisons indicate that the estimated total errors quoted at the end of Section 2.1 are approximately correct for all three datasets.

There is a simple reason for the excellent agreement between different j_* – M_* relations for disk-dominated galaxies. Most galactic disks are similar to each other over a wide radial range, with exponential surface density profiles and flat rotation curves, characterized by the radial scale R_d and the rotation velocity V_f , respectively. In the inner regions, the surface density profiles and rotation curves vary much more among galaxies, but these variations have little influence on the values of j_{*d} and M_{*d} . Thus, the relation, $j_{*d} = 2R_d V_f$, for an ideal disk with an exponential surface density profile and a flat rotation curve, is a good approximation for most real disks of giant spiral galaxies. This simplification makes the j_* – M_* relation for disk-dominated galaxies relatively easy to determine. Indeed, it has not changed much since the original derivation 35 years ago (Paper 0). The more difficult task is to determine the j_* – M_* relation for bulge-dominated galaxies.

The second conclusion apparent from Figure 1 is that there is a systematic offset between the Sweet et

al. (2018) j_* – M_* relation for disk-dominated CALIFA galaxies and the other three j_* – M_* relations for disk-dominated galaxies. When we fit Equation (1) to the galaxies with $\beta_* \leq 0.1$ in the Sweet et al. (2018) CALIFA sample, we obtain $\alpha = 0.56 \pm 0.14$ and $\log j_0 = 3.41 \pm 0.05$, essentially the same exponent as the other j_* – M_* relations, but a higher normalization by a factor of 2.0. Sweet et al. (2018) do not mention this offset in their paper. We suspect it arises from errors in their calculations of specific angular momentum, as discussed in the Appendix. In any case, the large, unexplained offset introduces a serious bias in the combined j_* – M_* relation Sweet et al. (2018) derived from the CALIFA, THINGS, and our Paper 1 datasets. This offset is one of the reasons Sweet et al. (2018) found a discrepant exponent ($\alpha \approx 1$) for disk-dominated galaxies. We discuss another reason in the Appendix.

The third conclusion apparent from Figure 1 is that our j_* – M_* relations for disk-dominated and bulge-dominated galaxies are roughly, but not exactly, parallel to each other. We quantify this impression by fitting Equation (1) to the galaxies in our sample with $\beta_* \geq 0.8$, i.e., essentially pure bulges (within the uncertainties in β_*), finding $\alpha = 0.83 \pm 0.16$ and $\log j_0 = 2.20 \pm 0.12$. Evidently, the j_* – M_* relation for bulge-dominated galaxies is slightly steeper than the one for disk-dominated galaxies, although the two exponents are consistent with each other at the $\sim 1.5\sigma$ level, while the normalizations differ by a factor of 7 ± 2 . The power-law fit for bulge-dominated galaxies presented here differs slightly from the one given in Paper 2, because the newer fit is based on a subsample of galaxies defined by a strict limit on bulge fraction, while the older one was based on a subsample comprised of all elliptical galaxies irrespective of their bulge fractions.

Unfortunately, we cannot compare our j_* – M_* scaling relation for bulge-dominated galaxies with other determinations, because none of the other samples includes enough high- β_* galaxies. We note that Cortese et al. (2016) found roughly parallel j_* – M_* relations for galaxies of different morphologies, ranging from early-type spirals to ellipticals, based on absorption-line kinematics derived from SAMI⁵ integral-field spectroscopy, in qualitative agreement with our results. However, the galaxies in the Cortese et al. (2016) sample lack disk–bulge decompositions and kinematic data that reach beyond $\sim 1R_e$, thus precluding a quantitative comparison with our results.

⁵ SAMI is an acronym for Sydney-AAO (Anglo-Australian Observatory) Multi-object Integral field spectrograph

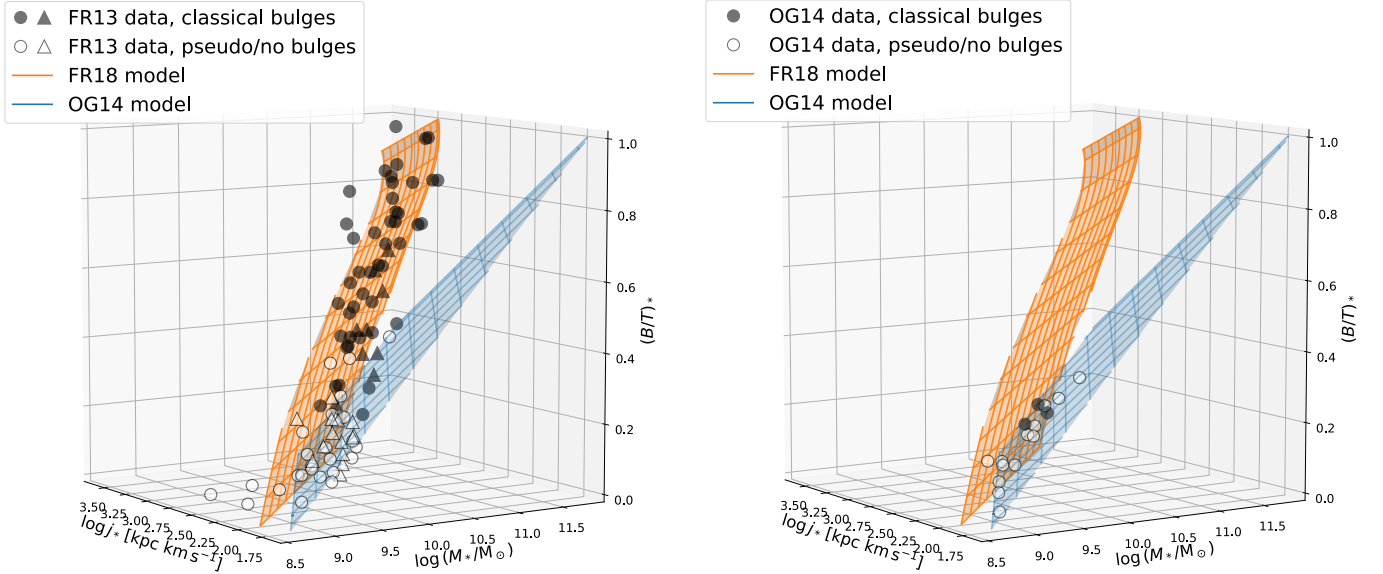


Figure 2. Stellar bulge fraction, $\beta_\star \equiv (B/T)_\star$, plotted against stellar specific angular momentum j_\star and stellar mass M_\star from our work (left panel) and from Obreschkow & Glazebrook (2014) (right panel). Filled symbols represent galaxies with classical bulges, and open symbols those with pseudo bulges or no bulges. For circles, the bulge classifications are more certain; for triangles, they are less certain. In both panels, the orange surface represents the relation for independent disks and bulges derived in the present study, while the blue plane represents the linear regression derived by Obreschkow & Glazebrook (2014).

3. 3D RELATIONS BETWEEN j_\star , M_\star , AND β_\star

We now examine the distribution of galaxies in the 3D space of specific angular momentum j_\star , mass M_\star , and bulge fraction β_\star . The j_\star – M_\star scaling relations discussed in the previous section are simply the projections of this distribution along the β_\star axis. We focus mainly on our own dataset, because it is the only one with full coverage in β_\star . However, we compare our results directly with those of Obreschkow & Glazebrook (2014) because they have made testable claims about the distribution of galaxies in $(\log j_\star, \log M_\star, \beta_\star)$ space. In the following, we disregard the Posti et al. (2018a) dataset because of its narrow coverage in β_\star and the Sweet et al. (2018) dataset for the reasons discussed in Section 2 and the Appendix.

The left and right panels of Figure 2 show the distribution of galaxies in $(\log j_\star, \log M_\star, \beta_\star)$ space for our sample and for the Obreschkow & Glazebrook (2014) sample, respectively. Galaxies with classical and pseudo bulges are distinguished in this diagram by filled and open symbols, respectively. Our sample has a mixture of classical and pseudo bulges, while the Obreschkow & Glazebrook (2014) sample is dominated by pseudo bulges. The galaxies in our sample lie on or near the curved orange surface, while those in the Obreschkow & Glazebrook (2014) sample lie on or near the blue plane. The orange surface and blue plane, which are replicated in both panels of Figure 2, differ substantially at high

bulge fraction, but converge toward each other at low bulge fraction. We elaborate on these similarities and differences in the remainder of this section.

The orange surface in Figure 2 is based on the following simple model inspired by the similar j_\star – M_\star scaling relations of galaxies with different β_\star shown in Figure 1. In this model, normal galaxies, in a first approximation, consist of a linear superposition of disks and bulges that follow separate scaling relations of the form $j_{\star d} = j_{0d}(M_{\star d}/M_0)^\alpha$ and $j_{\star b} = j_{0b}(M_{\star b}/M_0)^\alpha$, respectively (with $\log(M_0/M_\odot) = 10.5$ and all specific angular momenta expressed in units of kpc km s^{-1} , as before). Then the total values of specific angular momentum j_\star and mass M_\star for composite galaxies of any bulge fraction β_\star are related by

$$j_\star = (j_{\star d}M_{\star d} + j_{\star b}M_{\star b})/(M_{\star d} + M_{\star b}) = j_0(\beta_\star)(M_\star/M_0)^\alpha, \quad (2)$$

$$j_0(\beta_\star) = j_{0d}(1 - \beta_\star)^{\alpha+1} + j_{0b}\beta_\star^{\alpha+1}. \quad (3)$$

As expected, this j_\star – M_\star relation has the same exponent α for all values of β_\star , corresponding to parallel lines in the $\log j_\star$ – $\log M_\star$ diagram. The dependence of $\log j_\star$ on β_\star at fixed $\log M_\star$, however, is non-linear. Thus, in the 3D space of $\log j_\star$, $\log M_\star$, and β_\star , galaxies will lie on or near a curved 2D surface given by Equations (2) and (3) if they obey this simple model. It is easy to generalize this model to one in which the scaling relations

for disks and bulges have different exponents, α_d and α_b . We have not done this because it only complicates the analysis, without a commensurate gain in accuracy or insight, and because, with currently available data, α_d and α_b are statistically equal at the $\sim 1.5\sigma$ level according to our 2D fits in Section 2.2.

The orange surface in Figure 2 is our 3D fit of this simple model to our full dataset ($8.9 \leq \log(M_*/M_\odot) \leq 11.8$). In particular, we derive the best-fit values and 1σ errors of the parameters α , j_{0d} , and j_{0b} in Equations (2) and (3) by minimizing the trivariate χ^2 with the observations in the form $(\log j_*, \log M_*, \beta_*)$ and our estimates of the typical errors from Section 2.1. The results are $\alpha = 0.67 \pm 0.07$, $\log j_{0d} = 3.17 \pm 0.03$, $\log j_{0b} = 2.25 \pm 0.14$, and $\chi^2_{\text{red}} = 1.0$. The values of α and j_{0b} from this 3D fit are statistically the same as those from the 2D fits in Section 2.2 (within 1σ), while the value of $\log j_{0d}$ is 0.10 ± 0.04 higher. As expected, the single exponent α for all galaxies in the 3D fit lies between the separate values of α for disk-dominated and bulge-dominated galaxies in the 2D fits. The normalizations for disks and bulges (j_{0d} and j_{0b}) in the 3D fit differ by a factor of 8 ± 2 , slightly higher than in the 2D fits.

Two other features of this 3D fit are noteworthy. First, because the fit has $\chi^2_{\text{red}} = 1.0$, all the observed scatter can be accounted for by the estimated (total) errors, $\varepsilon(\log j_*)$, $\varepsilon(\log M_*)$, and $\varepsilon(\beta_*)$, with no need to invoke any intrinsic scatter. However, because these errors are only approximate, we cannot rule out even a fairly large intrinsic scatter, similar to the errors themselves. Second, the agreement between the model and our dataset is not simply a consequence of the fact that, in both cases, the total specific angular momentum and mass of galaxies (j_* , M_*) represent sums over the contributions from disks (j_{*d} , M_{*d}) and bulges (j_{*b} , M_{*b}). In the model, disks and bulges are assumed to follow separate scaling relations, with j_{*d} determined only by M_{*d} , and j_{*b} only by M_{*b} , whereas no such assumption was made in the empirical estimates of j_* and M_* . Moreover, for lenticular and elliptical galaxies, we estimated j_* and M_* directly from the overall surface brightness and stellar rotation profiles, without distinguishing the contributions from disks and bulges.

The blue plane in Figure 2 is the 3D linear regression by Obreschkow & Glazebrook (2014) to their dataset. They derived best-fit parameters (k_1 , k_2 , k_3) of the plane $\beta_* = k_1 \log M_* + k_2 \log j_* + k_3$ by minimizing the trivariate χ^2 with respect to the observations in the form $(\log j_*, \log M_*, \beta_*)$ and using their estimates of the typical errors. They then reexpressed these results in the form $j_* = j_0(\beta_*)(M_*/M_\odot)^\alpha$, analogous to our Equation (2), but with $j_0(\beta_*) = k \exp(-g\beta_*) \times 1000 \text{ kpc km s}^{-1}$,

in place of our Equation (3), and the parameter values $\alpha = 0.94 \pm 0.07$, $k = 0.89 \pm 0.11$, $g = 7.03 \pm 1.35$ (with $\log(M_0/M_\odot) = 10.0$). It is worth noting that this fit is not motivated by any underlying physical model; it is simply a convenient representation of the data. Moreover, the robustness of the fit is questionable, given that it is based on a small sample of galaxies ($N = 16$) with small bulge fractions ($\beta_* \leq 0.3$).

It is clear at a glance that the blue plane derived from the Obreschkow & Glazebrook (2014) dataset is not an acceptable fit to our dataset, especially for large bulge fractions. However, it is less obvious whether the orange surface derived from our dataset provides a good or bad fit to their dataset. This depends critically on the adopted errors in the χ^2 calculation. If we adopt the typical errors quoted by Obreschkow & Glazebrook (2014) of 0.02, 0.06, 0.02, respectively, for $\log j_*$, $\log M_*$, β_* , the fit is rejected by a wide margin. However, as discussed in Section 2 and the Appendix, these (partial) errors are unrealistically small. In particular, they are much smaller than the dispersions between independent estimates of these quantities by different authors. If instead, we adopt our estimates of the typical (total) errors from Section 2.1, we obtain $\chi^2_{\text{red}} = 0.9$, indicating an acceptable fit of the orange surface to the Obreschkow & Glazebrook (2014) dataset.

In Figure 3, we plot β_* against $\log(j_*/M_*^\alpha)$ with $\alpha = 0.67$ for both our dataset and the Obreschkow & Glazebrook (2014) dataset. This 2D projection of the 3D space of j_* , M_* , and β_* effectively removes the primary dependence of j_* on M_* from the scaling relation, thus highlighting its secondary dependence on β_* . The dashed curves in Figure 3, computed from Equations (2) and (3), are the projection of the orange surface in this direction. This representation shows even more clearly than Figure 2 that both datasets are consistent, within the scatter, with our simple model based on independent disks and bulges. Given the low χ^2_{red} , even the lone outlier in the Obreschkow & Glazebrook (2014) dataset is consistent with this model.

In Figures 2 and 3, we distinguish classical bulges from pseudo bulges by filled and open symbols, respectively. The bulge types for galaxies in our sample and the references from which they were taken, if available, are listed in Table 1. For 23 of the spirals, there are definite bulge classifications in the literature. Another 10 have no bulges, according to our adopted decompositions. The remaining 24 spirals either have no available bulge classifications, or have ambiguous types in the literature. We tentatively classify the bulges of these galaxies as “pseudo?” if they have $\beta_* < 0.2$ and “classical?” if they have $\beta_* > 0.2$, as suggested by the β_* -distributions of

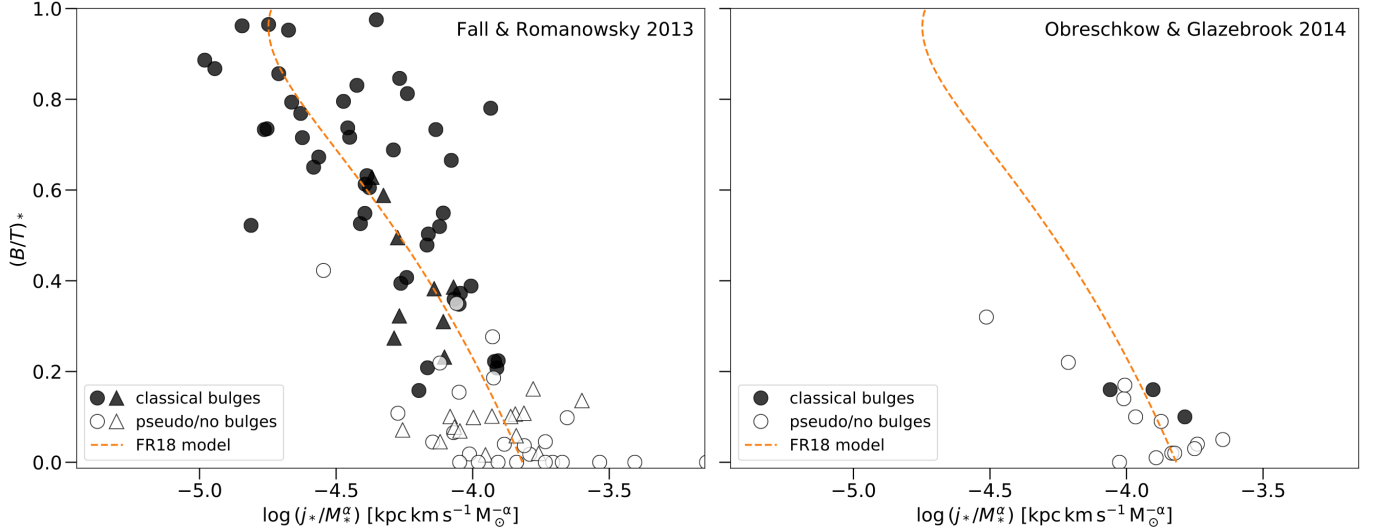


Figure 3. Stellar bulge fraction, $\beta_* \equiv (B/T)_*$, plotted against j_*/M_*^α with $\alpha = 0.67$ from our work (left panel) and from Obreschkow & Glazebrook (2014) (right panel). Filled symbols represent galaxies with classical bulges, and open symbols those with pseudo bulges or no bulges. For circles, the bulge classifications are more certain; for triangles, they are less certain. In both panels, the orange dashed line represents the relation for independent disks and bulges derived in the present study. Note that galaxies with pseudo bulges cluster at the lower end of this relation.

galaxies with definite bulge types. In Figures 2 and 3, galaxies with more certain bulge types are indicated by circles, while those with less certain bulge types are indicated by triangles.

It is worth noting here that the definition, observational signatures, and physical origins of pseudo bulges are not universally agreed upon (see Kormendy & Kennicutt 2004 for a review). For some authors, pseudo bulges are flattened (disk-like) structures in the inner parts of galaxies for which the surface brightness profile exceeds that of a fitted exponential disk. For others, they are bulges for which the fitted surface brightness profile has a low Sérsic index (typically, $n < 2$), irrespective of whether they have flat or round 3D shapes. For still others, pseudo bulges are whatever structures may result from the “secular” re-arrangement of material in the inner parts of galactic disks by bars and/or oval distortions, including heating in the vertical direction. Evidently, there is no consensus on even such a basic property of pseudo bulges as their 3D shapes. These ambiguities complicate any attempts to discern whether classical and pseudo bulges follow the same or different j_* – M_* scaling relations and to interpret such results astrophysically.

With these caveats in mind, we note from Figure 2, and especially Figure 3, the strong tendency for galaxies with classical and pseudo bulges to be segregated from each other above and below $\beta_* \sim 0.2$. At the same time, they appear to span *different parts* of the *same*

surface in $(\log j_*, \log M_*, \beta_*)$ space. In particular, they are both consistent, within the scatter, with our simple model based on independent disks and bulges, with $\chi^2_{\text{red}} = 0.7$ for classical bulges and $\chi^2_{\text{red}} = 1.2$ for pseudo bulges. In any case, there is no statistically significant indication, from either our dataset or the Obreschkow & Glazebrook (2014) dataset, that galaxies with classical and pseudo bulges lie on fundamentally different 2D surfaces in the 3D space of j_* , M_* , and β_* . The scatter in the observations is large enough, however, that we cannot rule out subtle differences in these distributions.

4. SUMMARY AND DISCUSSION

The main conclusion of this paper is that the observed values of specific angular momentum j_* , mass M_* , and bulge fraction β_* of the stellar parts of most normal galaxies are consistent, in a first approximation, with a simple model based on a linear superposition of independent disks and bulges. The disks and bulges in this model follow scaling relations of the form $j_{*d} \propto M_{*d}^\alpha$ and $j_{*b} \propto M_{*b}^\alpha$ with $\alpha = 0.67 \pm 0.07$ but offset from each other by a factor of 8 ± 2 over the mass range $8.9 \leq \log(M_*/M_\odot) \leq 11.8$. Separate fits for disks and bulges alone give $\alpha = 0.58 \pm 0.10$ and $\alpha = 0.83 \pm 0.16$, respectively. This simple model correctly predicts that galaxies will lie on or near a curved 2D surface specified by Equations (2) and (3) in the 3D space of $\log j_*$, $\log M_*$, and β_* . These results reinforce and extend our earlier suggestion that the distribution of galaxies with different β_* in the j_* – M_* diagram constitutes an objec-

tive, physically motivated alternative to subjective classification schemes such as the Hubble sequence.

For disk-dominated galaxies in the mass range considered here, the j_\star – M_\star scaling relation is now quite secure, as shown in Figure 1 by the excellent agreement between our determination (from Paper 2) and those of Obreschkow & Glazebrook (2014) and Posti et al. (2018a). Two factors contribute to the robustness of this scaling relation. First, no special efforts are required to obtain photometric and kinematic data that extend to large enough radii (in units of R_e) to estimate reliably the disk contributions $j_{\star d}$ and $M_{\star d}$ to the total values j_\star and M_\star , which usually turn out to be close to those for ideal disks with exponential surface density profiles and flat rotation curves. Second, any uncertainties in the bulge contributions $j_{\star b}$ and $M_{\star b}$, even when substantial, have only a minor impact on the total values j_\star and M_\star .

For most of the giant galaxies studied here, cold gas (HI and H₂) makes a relatively small contribution to their specific angular momentum and mass, and the stellar j_\star – M_\star scaling relation is a good proxy for the baryonic j_{bary} – M_{bary} scaling relation (Obreschkow & Glazebrook 2014).⁶ This is no longer true, however, for gas-rich dwarf galaxies, which contain more specific angular momentum and mass in cold gas than in stars. Several recent studies have extended the j_{bary} – M_{bary} scaling relation down into the mass range $7 \lesssim \log(M_{\text{bary}}/M_\odot) \lesssim 9$, with somewhat confusing claims about whether it lies above or matches onto the extrapolated j_{bary} – M_{bary} and j_\star – M_\star scaling relations from higher masses (Butler et al. 2017; Chowdhury & Chengalur 2017; Elson 2017; Kurapati et al. 2018). Continuing and refining this work is important, because it has the potential to place constraints on the mass dependence of the retained or sampled fraction of specific angular momentum in galaxies f_j (see below).

For bulge-dominated galaxies, the j_\star – M_\star scaling relation is based almost entirely on our work. In this case, the main challenge is obtaining kinematic data that extend to large enough radii (in units of R_e) that the estimates of $j_{\star b}$ have converged. This is important because the stellar rotation profiles of bulge-dominated galaxies, unlike the H α and HI rotation curves of disk-dominated galaxies, exhibit a great variety of behaviors; some are flat, while others rise or fall. All of our estimates of

$j_{\star b}$ are based on kinematic data that extend to $\sim 2R_e$ and some to much larger radii, thus capturing as much angular momentum with as little extrapolation as possible. Nevertheless, additional studies of the j_\star – M_\star scaling relation for spheroid-dominated galaxies, based on 2D kinematic data that reach even larger radii (for example, $R > 5R_e$), would certainly be desirable.

For intermediate-type galaxies, the main challenge to deriving the j_\star – M_\star scaling relation is in disentangling the contributions to j_\star and M_\star from the superposed disks and bulges. The specific angular momenta of bulges in such galaxies have been approximated in three different ways, by assuming that their rotation velocity is either (1) zero, (2) the same as the rotation velocity of their associated disks, or (3) the same as the mean rotation velocity for bulges of the same velocity dispersion and ellipticity. Method (1) and (2) clearly lead to systematic under- and overestimates of $j_{\star b}$, respectively, while method (3), the one we have adopted, contributes some scatter but little if any bias to the j_\star – M_\star scaling relation. More accurate results will require careful modeling of extensive 2D photometric and kinematic data to disentangle the velocity fields and hence the specific angular momenta of superposed disks and bulges (as in the recent work of Rizzo et al. (2018) on lenticular galaxies).

The bulge fraction β_\star is inherently uncertain because it depends on the adopted method for decomposing galaxies into disks and bulges, either by pre-specifying their 3D shapes (flat versus round) or by pre-specifying their surface brightness profiles (exponential versus Sérsic). These two methods generally give similar values of β_\star for bulge-dominated galaxies (elliptical, lenticulars, and early-type spirals), but they can give substantially different values of β_\star for disk-dominated galaxies (late-type spirals). A related complication is the lack of consensus on the definition of pseudo bulges, including whether they must always be flat (like disks) or may sometimes be round (like spheroids). This ambiguity adds substantially to the uncertainty in estimates of β_\star for disk-dominated galaxies, where pseudo bulges are much more common than classical bulges.

We find no statistically significant indication that galaxies with pseudo bulges and classical bulges follow different relations in the space of $\log j_\star$, $\log M_\star$, and β_\star . This does not mean that both types of galaxies follow exactly the same relation, of course, merely that any differences must be small enough to hide within the scatter. Obreschkow & Glazebrook (2014) found a different relation (with $\alpha \approx 1$) from a small sample of spiral galaxies with a preponderance of pseudo bulges (13/16) covering a narrow range in β_\star . This result, however, is based on adopted (partial) errors in j_\star , M_\star , and β_\star that ne-

⁶ The baryonic scaling relations mentioned here include only stars and cold gas, not the warm and hot diffuse gas in galactic halos, which might actually dominate the total j_{bary} and M_{bary} budgets of some galaxies.

glect the inherent uncertainties mentioned above and are therefore unrealistically small. As we have shown here, the statistical significance of the Obreschkow & Glazebrook (2014) relation disappears when we adopt more realistic (total) errors in these quantities. Sweet et al. (2018) also found a different relation (again with $\alpha \approx 1$), based on a dataset with large systematic errors in j_* .

Finally, we offer a few remarks on the astrophysical implications of our results, following the precepts of Paper 1. Comparing the scaling relation for the stellar components of galaxies in the form $j_* = j_0(M_*/M_0)^\alpha$ with that for dark-matter halos in the standard Λ CDM cosmology, we derive the relation $f_j/f_M^{2/3} = 6.8(j_0/10^3 \text{ kpc km s}^{-1})(M_*/M_0)^{\alpha-2/3}$ between the fractions of specific angular momentum and mass in stars relative to dark matter, $f_j \equiv j_*/j_{\text{halo}}$ and $f_M \equiv M_*/M_{\text{halo}}$ (with $M_0 = 10^{10.5} M_\odot$ again). With the exponent α and normalizations j_0 from our 3D fit to Equations (2) and (3), this relation becomes $f_j/f_M^{2/3} = 10.0 \pm 0.6$ for disks and $f_j/f_M^{2/3} = 1.2 \pm 0.4$ for bulges. Then, with the separate relations between f_M and M_* for late-type and early-type galaxies from Dutton et al. (2010), we obtain $f_j \approx 1.0$ for disks and $f_j \approx 0.1$ for bulges at $M_* \sim 10^{10.5} M_\odot$ and only mild variations over the range $10^{9.5} M_\odot \lesssim M_* \lesssim 10^{11.5} M_\odot$. These estimates of f_j differ slightly from the ones derived in Paper 2 for the same dataset because the new 3D and old 2D fits return slightly different values of j_0 .

The relations $f_j/f_M^{2/3} = \text{constant}$ derived above imply that f_j and f_M must have qualitatively similar dependences on M_* , namely a broad peak near $M_* \sim 10^{10.5} M_\odot$, a shallow decline to lower M_* , and a somewhat steeper decline to higher M_* . This is why we find only mild variations in f_j . Recent analyses by other authors also indicate $f_j \approx \text{constant}$ near $M_* \sim 10^{10.5} M_\odot$ (see Fig. 12 of Lapi et al. 2018b and Fig. 3 of Posti et al. 2018a). Over much wider mass ranges, the deviations from a constant f_j may become more pronounced. The model of disk formation preferred by Posti et al. (2018a) has $f_j \propto f_M^s \propto M_*^\gamma$ with $\gamma = s(2 - 3\alpha)/(2 - 3s)$, which, when fitted to their full dataset ($10^{7.0} M_\odot \leq M_* \leq 10^{11.3} M_\odot$), gives $\alpha = 0.59 \pm 0.02$, $s = 0.4 \pm 0.1$, and thus $\gamma = 0.12 \pm 0.03$. However, even this weak dependence of f_j on mass could be erased if the $j_{\text{bary}}-M_{\text{bary}}$ relation for gas-rich dwarf galaxies turns out to be shallower than the j_*-M_* relation by only $\Delta\alpha \approx 0.15$ (again, see Fig. 3 of Posti et al. 2018a). This is why it is important to refine estimates of the baryonic relation at low masses.

The fractions f_j and f_M for disks and bulges and the corresponding $j-M$ scaling relations (stellar and bary-

onic) are potentially determined by a large number of astrophysical processes. These include tidal torques, dynamical friction of baryonic structures within dark-matter halos, shocks and radiative cooling in the interstellar and circumgalactic media, star formation and its associated feedback, inflow, outflow, and recycling of gas, merging of gas clumps and dwarf galaxies, and tidal stripping of the outer parts of halos and their circumgalactic media by neighboring halos. We reviewed these processes and their potential impact on the $j-M$ scaling relations for disks and bulges at some length in Paper 1. Here, we note only the growing interest in biased-collapse models in which the fractions f_j and f_M are determined by the hypotheses that the baryons and dark matter in protogalaxies start with similar distributions of specific angular momentum and mass and that, at any given time, only the baryons within some critical radius are able to collapse and form the visible parts of galaxies. Analytical models of this type and their implications for the $j-M$ scaling relations are explored in several recent papers (Shi et al. 2017; Lapi et al. 2018a; Posti et al. 2018a, 2018b; see also Paper 1 and references therein).

In the past few years, hydrodynamical simulations of forming galaxies have succeeded in reproducing, at least approximately, the observed $j-M$ scaling relations (Genel et al. 2015; Pedrosa & Tissera 2015; Teklu et al. 2015; Agertz & Kravtsov 2016; Zavala et al. 2016; DeFelippis et al. 2017; Grand et al. 2017; Lagos et al. 2017; Sokołowska et al. 2017; Stevens et al. 2017; El-Badry et al. 2018; Lagos et al. 2018; Obreja et al. 2018). One of the main lessons from these simulations is that feedback is an essential ingredient to match the observed relations for both disk-dominated and spheroid-dominated galaxies. Without feedback, the simulations suffer from the well-known overcooling and angular momentum problems and fail to produce the full range of galactic morphologies. Another important ingredient is merging, which appears to explain, at least partially, the slow rotation of spheroids relative to disks.

Despite the success of recent analytical models and hydrodynamical simulations, we do not yet have definitive answers to some important theoretical questions about the $j-M$ scaling relations, such as the following. Given the potential complexity of galaxy formation, why are the observed $j-M$ relations so simple? In particular, why are the specific angular momentum and mass fractions f_j and f_M so closely linked that they result in power-law $j-M$ relations over 3–4 decades in mass (at least for disks)? Why do the disks of massive galaxies have nearly the same specific angular momentum as their dark-matter halos ($f_j \sim 1.0$) and why do their

bulges have much less ($f_j \sim 0.1$)? Answering these questions will require a better understanding of how much the specific angular momentum of mass elements inside forming galaxies is redistributed and which physical mechanisms are most responsible for this redistribution. This is a promising direction for future analysis of hydro-

dynamical simulations (as already begun by DeFelippis et al. 2017).

We thank Kenneth Freeman and John Kormendy for guiding us through the mysteries of pseudo bulges. This research was supported in part by the National Science Foundation through grants AST16-16710 and PHY17-48958. AJR is a Research Corporation for Science Advancement Cottrell Scholar.

REFERENCES

- Agertz, O., & Kravtsov, A. V. 2016, *ApJ*, 824, 79
- Alcorn, L. Y., Tran, K.-V., Glazebrook, K., et al. 2018, *ApJ*, 858, 47
- Balcells, M., Graham, A. W., & Peletier, R. F. 2007, *ApJ*, 665, 1084
- Burkert, A., Förster Schreiber, N. M., Genzel, R., et al. 2016, *ApJ*, 826, 214
- Butler, K. M., Obreschkow, D., & Oh, S.-H. 2017, *ApJL*, 834, L4
- Chowdhury, A., & Chengalur, J. N. 2017, *MNRAS*, 467, 3856
- Contini, T., Epinat, B., Bouché, N., et al. 2016, *A&A*, 591, A49
- Cortese, L., Fogarty, L. M. R., Bekki, K., et al. 2016, *MNRAS*, 463, 170
- Cortesi, A., Merrifield, M. R., Coccato, L., et al. 2013, *MNRAS*, 432, 1010
- Dalcanton, J. J., Spergel, D. N., & Summers, F. J. 1997, *ApJ*, 482, 659
- DeFelippis, D., Genel, S., Bryan, G. L., & Fall, S. M. 2017, *ApJ*, 841, 16
- de Souza, R. E., Gadotti, D. A., & dos Anjos, S. 2004, *ApJS*, 153, 411
- Dutton, A. A., Conroy, C., van den Bosch, F. C., Prada, F., & More, S. 2010, *MNRAS*, 407, 2
- El-Badry, K., Quataert, E., Wetzel, A., et al. 2018, *MNRAS*, 473, 1930
- Elson, E. C. 2017, *MNRAS*, 472, 4551
- Fabricius, M. H., Saglia, R. P., Fisher, D. B., Drory, N., Bender, R., & Hopp, U. 2012, *ApJ*, 754, 67
- Falcón-Barroso, J., Lyubenova, M., van de Ven, G., et al. 2017, *A&A*, 597, A48
- Fall, S. M. 1983, in *IAU Symp. 100, Internal Kinematics and Dynamics of Galaxies*, ed. E. Athanassoula (Cambridge: Cambridge Univ. Press), 391 (Paper 0)
- Fall, S. M., & Efstathiou, G. 1980, *MNRAS*, 193, 189
- Fall, S. M., & Romanowsky, A. J. 2013, *ApJL*, 769, L26 (Paper 2)
- Fernández Lorenzo, M., Sulentic, J., Verdes-Montenegro, L., et al. 2014, *ApJL*, 788, L39
- Fisher, D. B., & Drory, N. 2008, *AJ*, 136, 773
- Fisher, D. B., & Drory, N. 2010, *ApJ*, 716, 942
- Fisher, D. B., & Drory, N. 2011, *ApJL*, 733, L47
- Gao, H., & Ho, L. C. 2017, *ApJ*, 845, 114
- Genel, S., Fall, S. M., Hernquist, L., et al. 2015, *ApJL*, 804, L40
- Grand, R. J. J., Gómez, F. A., Marinacci, F., et al. 2017, *MNRAS*, 467, 179
- Harrison, C. M., Johnson, H. L., Swinbank, A. M., et al. 2017, *MNRAS*, 467, 1965
- Huang, K.-H., Fall, S. M., Ferguson, H. C., et al. 2017, *ApJ*, 838, 6
- Kawamata, R., Ishigaki, M., Shimasaku, K., Oguri, M., & Ouchi, M. 2015, *ApJ*, 804, 103
- Kawamata, R., Ishigaki, M., Shimasaku, K., Oguri, M., Ouchi, M., & Tanigawa, S. 2018, *ApJ*, 855, 4
- Kent, S. M. 1986, *AJ*, 91, 1301
- Kent, S. M. 1987, *AJ*, 93, 816
- Kent, S. M. 1988, *AJ*, 96, 514
- Kormendy, J., & Bender, R. 2011, *Nature*, 469, 377
- Kormendy, J., Bender, R., & Cornell, M. E. 2011, *Nature*, 469, 374
- Kormendy, J., & Kennicutt, R. C. 2004, *ARA&A*, 42, 603
- Kravtsov, A. V. 2013, *ApJL*, 764, L31
- Kurapati, S., Chengalur, J. N., Pustilnik, S., & Kamphuis, P. 2018, *MNRAS*, 479, 228
- Lagos, C. del P., Stevens, A. R. H., Bower, R. G., et al. 2018, *MNRAS*, 473, 4956
- Lagos, C. del P., Theuns, T., Stevens, A. R. H., et al. 2017, *MNRAS*, 464, 3850
- Lapi, A., Pantoni, L., Zanisi, L., et al. 2018a, *ApJ*, 857, 22
- Lapi, A., Salucci, P., & Danese, L. 2018b, *ApJ*, 859, 2
- Lelli, F., McGaugh, S. S., Schombert, J. M. 2016, *AJ*, 152, 157
- Leroy, A. K., Walter, F., Brinks, E., et al. 2008, *AJ*, 136, 2782
- Méndez-Abreu, J., Aguerri, J. A. L., Falcón-Barroso, J., et al. 2018, *MNRAS*, 474, 1307
- Méndez-Abreu, J., Ruiz-Lara, T., Sánchez-Menguiano, L., et al. 2017, *A&A*, 598, A32
- Mo, H. J., Mao, S., & White, S. D. M. 1998, *MNRAS*, 295, 319
- Möllenhoff, C. 2004, *A&A*, 415, 63
- Neumann, J., Wisotzki, L., Choudhury, O. S., et al. 2017, *A&A*, 604, A30
- Obreja, A., Dutton, A. A., Macciò, A. V., et al. 2018, *MNRAS*, submitted (arXiv:1804.06635)
- Obreschkow, D., & Glazebrook, K. 2014, *ApJ*, 784, 26
- Okamura, T., Shimasaku, K., & Kawamata, R. 2018, *ApJ*, 854, 22
- Pedrosa, S. E., & Tissera, P. B. 2015, *A&A*, 584, A43
- Posti, L., Fraternali, F., Di Teodoro, E. M., & Pezzulli, G. 2018a, *A&A*, 612, L6
- Posti, L., Pezzulli, G., Fraternali, F., & Di Teodoro, E. M. 2018b, *MNRAS*, 475, 232
- Rizzo, F., Fraternali, F., & Iorio, G. 2018, *MNRAS*, 476, 2137
- Romanowsky, A. J., & Fall, S. M. 2012, *ApJS*, 203, 17 (Paper 1)
- Schulze, F., Remus, R.-S., Dolag, K., Burkert, A., Emsellem, E., & van de Ven, G. 2018, *MNRAS*, 480, 4636
- Shi, J., Lapi, A., Mancuso, C., Wang, H., & Danese, L. 2017, *ApJ*, 843, 105
- Shibuya, T., Ouchi, M., & Harikane, Y. 2015, *ApJS*, 219, 15
- Sokołowska, A., Capelo, P. R., Fall, S. M., Mayer, L., Shen, S., & Bonoli, S. 2017, *ApJ*, 835, 289
- Stevens, A. R. H., Croton, D. J., & Mutch, S. J. 2016, *MNRAS*, 461, 859
- Stevens, A. R. H., Lagos, C. del P., Contreras, S., et al. 2017, *MNRAS*, 467, 2066
- Sweet, S. M., Fisher, D., Glazebrook, K., Obreschkow, D., Lagos, C., & Wang, L. 2018, *ApJ*, 860, 37
- Swinbank, A. M., Harrison, C. M., Trayford, J., et al. 2017, *MNRAS*, 467, 3140
- Tadaki, K.-I., Genzel, R., Kodama, T., et al. 2017, *ApJ*, 834, 135
- Teklu, A. F., Remus, R.-S., Dolag, K., et al. 2015, *ApJ*, 812, 29
- Walcher, C. J., Wisotzki, L., Bekeraité, B., et al. 2014, *A&A*, 569, A1
- Walter, F., Brinks, E., de Blok, W. J. G., et al. 2008, *AJ*, 136, 2563
- Weinzirl, T., Jogee, S., Khochfar, S., Burkert, A., & Kormendy, J. 2009, *ApJ*, 696, 411
- Zavala, J., Frenk, C. S., Bower, R., et al. 2016, *MNRAS*, 460, 4466
- Zoldan, A., De Lucia, G., Xie, L., Fontanot, F., & Hirschmann, M. 2018, *MNRAS*, 481, 1376

Table 1. Specific Angular Momenta, Masses, and Bulge Fractions of Sample Galaxies

Name	Galaxy type	$\log_{10} M_{\star}$ [M_{\odot}]	$\log_{10} j_{\star}$ [kpc km s $^{-1}$]	β_{\star}	Bulge type	Reference
(1)	(2)	(3)	(4)	(5)	(6)	(7)
NGC 224	Sb	10.91	3.34	0.22	classical	KK04, FD11
NGC 247	Sd	9.47	2.90	0.00	none	FD11
NGC 300	Sd	8.95	2.42	0.00	none	FD11
NGC 701	Sc	10.20	2.74	0.00	none	–
NGC 753	Sbc	11.00	3.27	0.07	pseudo?	–
NGC 801	Sc	11.30	3.60	0.28	pseudo	KB11
NGC 821	E6	10.94	2.53	0.73	classical	dS+04
NGC 1023	S0	10.92	3.19	0.67	classical	K+11, F+12, C+13
NGC 1024	Sab	11.21	3.32	0.38	classical?	–
NGC 1087	Sc	10.25	2.91	0.00	none	–
NGC 1316	S0	11.85	3.64	0.81	classical	dS+04
NGC 1325	Sbc	10.35	3.16	0.05	pseudo	FD08
NGC 1339	E3	10.44	2.81	0.73	classical	–
NGC 1344	E4	11.05	2.59	0.73	classical	–
NGC 1353	Sbc	10.65	3.04	0.15	pseudo	KK04, FD08
NGC 1357	Sab	10.92	3.22	0.37	classical	GH17
NGC 1373	E2	9.71	1.62	0.96	classical	–
NGC 1379	E0	10.60	2.08	0.89	classical	–
NGC 1380	S0	11.27	3.45	0.35	classical	–
NGC 1381	S0	10.68	3.10	0.39	classical	–
NGC 1400	S0	10.99	2.37	0.87	classical	–
NGC 1404	E1	11.18	3.02	0.83	classical	–
NGC 1407	E0	11.58	3.03	0.95	classical	–
NGC 1417	Sb	11.05	3.51	0.11	pseudo?	–
NGC 1421	Sbc	10.42	3.33	0.14	pseudo?	–
NGC 1620	Sbc	11.08	3.51	0.10	pseudo?	–
NGC 2310	S0	10.25	2.91	0.21	classical	–
NGC 2403	Scd	9.58	2.70	0.00	none	–
NGC 2577	S0	10.75	3.08	0.35	classical	–
NGC 2590	Sbc	11.17	3.33	0.31	classical?	–
NGC 2592	E2	10.68	3.00	0.55	classical	MA+18
NGC 2608	Sb	10.44	2.86	0.10	pseudo?	–
NGC 2639	Sa	11.24	3.11	0.63	classical?	–
NGC 2699	E1	10.47	2.59	0.61	classical	–
NGC 2708	Sb	10.63	3.14	0.10	pseudo?	–
NGC 2715	Sc	10.46	3.20	0.02	pseudo?	–

Table 1 continued

Table 1 (*continued*)

Name	Galaxy type	$\log_{10} M_{\star}$ [M_{\odot}]	$\log_{10} j_{\star}$ [kpc km s $^{-1}$]	β_{\star}	Bulge type	Reference
(1)	(2)	(3)	(4)	(5)	(6)	(7)
NGC 2742	Sc	10.33	3.08	0.02	pseudo	M04
NGC 2768	S0	11.28	3.57	0.78	classical	C+13
NGC 2775	Sab	11.22	3.30	0.21	classical	W+09, F+12
NGC 2778	E2	10.18	2.66	0.52	classical	–
NGC 2815	Sb	11.08	3.30	0.39	classical?	–
NGC 2841	Sb	10.99	3.05	0.39	classical	F+12
NGC 2844	Sa	10.16	2.66	0.23	classical?	–
NGC 2903	Sbc	10.49	3.00	0.00	none	–
NGC 2998	Sc	10.79	3.37	0.04	pseudo	KB11
NGC 3031	Sab	10.85	3.02	0.16	classical	KK04, F+12
NGC 3067	Sab	10.35	2.77	0.05	pseudo?	–
NGC 3115	S0	10.98	3.14	0.50	classical	FD08, K+11, C+13
NGC 3156	S0	10.08	2.47	0.41	classical	–
NGC 3198	Sc	10.11	3.02	0.00	none	–
NGC 3200	Sc	11.13	3.62	0.16	pseudo?	–
NGC 3203	S0	10.84	3.30	0.22	classical	–
NGC 3377	E5	10.42	2.53	0.53	classical	–
NGC 3379	E2	10.88	2.53	0.86	classical	–
NGC 3593	S0/a	9.78	2.25	0.07	pseudo?	KB11, S+18
NGC 3605	E3	10.01	2.28	0.63	classical	–
NGC 3898	Sab	10.98	3.01	0.69	classical	F+12
NGC 4062	Sc	10.02	2.78	0.04	pseudo	FD08, W+09
NGC 4236	Sdm	8.91	2.78	0.00	none	–
NGC 4258	Sbc	10.85	3.38	0.00	none	–
NGC 4318	E3	9.78	2.12	0.55	classical	–
NGC 4374	E1	11.60	3.37	0.98	classical	–
NGC 4378	Sa	11.37	3.29	0.49	classical?	–
NGC 4387	E4	10.17	2.19	0.65	classical	–
NGC 4419	Sa	10.32	2.59	0.11	pseudo	FD10
NGC 4434	E1	10.32	2.24	0.77	classical	–
NGC 4448	Sab	9.96	2.51	0.22	pseudo	F+12
NGC 4464	S0	9.85	1.74	0.52	classical	–
NGC 4478	E2	10.39	2.25	0.79	classical	–
NGC 4494	E1	11.00	2.85	0.80	classical	–
NGC 4551	E3	10.14	2.13	0.72	classical	–
NGC 4564	E5	10.44	2.78	0.48	classical	FD08, K+11
NGC 4594	Sa	11.49	3.38	0.85	classical	KK04, FD11
NGC 4605	Sc	9.25	2.14	0.02	pseudo	FD10

Table 1 continued

Table 1 (*continued*)

Name	Galaxy type	$\log_{10} M_{\star}$ [M_{\odot}]	$\log_{10} j_{\star}$ [kpc km s $^{-1}$]	β_{\star}	Bulge type	Reference
(1)	(2)	(3)	(4)	(5)	(6)	(7)
NGC 4697	E4	10.94	2.72	0.67	classical	–
NGC 4698	Sab	10.85	2.89	0.59	classical?	KB11, F+12
NGC 4736	Sab	10.60	2.51	0.42	pseudo	KK04, F+12
NGC 4845	Sab	10.98	3.24	0.08	pseudo?	–
NGC 5033	Sc	10.97	3.38	0.19	pseudo	FD10
NGC 5055	Sbc	10.92	3.19	0.07	pseudo	F+12
NGC 5128	S0	11.21	3.01	0.72	classical	–
NGC 5846	E1	11.40	2.84	0.96	classical	–
NGC 6314	Sa	11.31	3.07	0.74	classical	N+17
NGC 7171	Sb	10.59	3.21	0.06	pseudo?	dS+04
NGC 7217	Sab	10.96	3.00	0.27	classical?	KB11, F+12
NGC 7331	Sb	11.17	3.16	0.32	classical?	KK04, F+12
NGC 7537	Sbc	10.11	2.67	0.35	pseudo	B+07
NGC 7541	Sbc	10.95	3.33	0.02	pseudo?	–
NGC 7606	Sb	11.17	3.44	0.10	pseudo?	–
NGC 7617	S0	10.74	2.75	0.61	classical	–
NGC 7664	Sc	10.61	2.91	0.04	pseudo	FL+14
IC 467	Sc	10.15	3.02	0.00	none	–
UGC 11810	Sbc	10.45	3.30	0.10	pseudo	FL+14
UGC 12810	Sc	11.00	3.51	0.11	pseudo?	–

NOTE— This table is a revision of Tables 3–5 in Paper 1 with the values of M_{\star} , j_{\star} , and β_{\star} calculated as described in Paper 2. Galaxies with missing colors or peculiar types are not included here. Bulge types followed by a question mark are uncertain, as discussed in Section 3. References for bulge types are abbreviated as follows. B+07: Balcells et al. (2007); C+13: Cortesi et al. (2013); dS+04: de Souza et al. (2004); FD08: Fisher & Drory (2008); FD10: Fisher & Drory (2010); FD11: Fisher & Drory (2011); F+12: Fabricius et al. (2012); FL+14: Fernández Lorenzo et al. (2014); GH17: Gao & Ho (2017); K+11: Kormendy et al. (2011); KB11: Kormendy & Bender (2011); KK04: Kormendy & Kennicutt (2004); M04: Möllenhoff (2004); MA+18: Méndez-Abreu et al. (2018); N+17: Neumann et al. (2017); S+18: Sweet et al. (2018); W+09: Weinzierl et al. (2009).

APPENDIX

A. ERRORS IN j_* , M_* , AND β_*

The purpose of this appendix is to provide some further insight into both random and systematic errors in the stellar specific angular momentum j_* , mass M_* , and bulge fraction β_* . We begin by comparing the independent estimates of these quantities by different authors for the 6–10 galaxies in common between our dataset and those of Obreschkow & Glazebrook (2014) and Posti et al. (2018a). These are plotted against each other in Figure 4. Evidently, the correlations between the different estimates are nearly linear, apart from a tendency by Posti et al. (2018a) to assign $\beta_* = 0$ to galaxies with small bulges. The mean offsets are $\Delta \log j_* = 0.06$, $\Delta \log M_* = 0.06$, and $\Delta \beta_* = 0.10$, and the one-sample dispersions (i.e., two-sample dispersions divided by $\sqrt{2}$) about them are $\sigma(\log j_*) = 0.11$, $\sigma(\log M_*) = 0.10$, and $\sigma(\beta_*) = 0.09$. These results are consistent with our estimates of the total errors $\varepsilon(\log j_*)$, $\varepsilon(\log M_*)$, and $\varepsilon(\beta_*)$ quoted at the end of Section 2.1.

The different methods of disk–bulge decomposition can lead to discrepancies in the derived values of β_* , especially for pseudo bulges. In the method pioneered by Kent (1986), decomposition is based on the fundamental physical distinction between flat (rotation-supported) disks and round (dispersion-supported) bulges. In the more familiar method, decomposition is based on imposed templates for the surface brightness profiles: exponential for disks and Sérsic for bulges. However, it is important to recognize that there is no fundamental physical justification for imposed templates of exactly these forms, from either cosmology or stellar dynamics. The different values of β_* returned by the two decomposition methods mostly reflect the fact that real bulges have a variety of 3D shapes and surface brightness profiles, rather than measurement errors. Fortunately, both methods usually give similar values of the radial scale of the disk R_d , typically within $\sim 10\%$, and hence similar values of the disk contribution to j_* . (See Section 4.1 of Paper 1 for a more complete discussion of this issue.)

As noted in Section 2.2, the CALIFA part of the Sweet et al. (2018) j_* – M_* relation for disk-dominated galaxies has the same exponent ($\alpha \approx 0.6$) as the others plotted in Figure 1 but is higher by a factor of about 2. We do not know the full reason for this offset, but we have found some clues. When we estimate M_* for some of the CALIFA galaxies by our own methods, we usually obtain results within ~ 0.1 dex of those adopted by Sweet et al. (2018) from Falcón-Barroso et al. (2017). For disk-dominated CALIFA galaxies, the estimates of specific angular momentum j_* , radial scale R_d , and rotation velocity V_f listed in Table 1 of Sweet et al. (2018) are typically related by $j_* \sim 5R_d V_f$, i.e., about 2.5 times the value of j_* for an ideal disk with an exponential surface density profile and a flat rotation curve, which is known to be a good approximation for most real disks. Thus, we strongly suspect that the Sweet et al. (2018) estimates of j_* suffer from some systematic error of roughly the amount needed to account for the offset between the CALIFA and the other j_* – M_* relations.

In the process of combining datasets to derive their published j_* – M_* relation, Sweet et al. (2018) introduced another systematic error. They made a non-linear rescaling of all our estimates of specific angular momentum of the form $j_* \rightarrow j_*^{1.3}$, based on a claim by Obreschkow & Glazebrook (2014). If valid, this would induce a corresponding change $\alpha \rightarrow 1.3\alpha$, hence $\alpha \approx 0.6 \rightarrow 0.8$, in the exponent of the power law $j_* \propto M_*^\alpha$. This, in turn, would spoil the excellent agreement between the j_* – M_* scaling relations for disk-dominated galaxies from our work (Paper 2), Obreschkow & Glazebrook (2014), and Posti et al. (2018a) shown in Figure 1, and therefore can be ruled out on this basis alone. Furthermore, the Sweet et al. (2014) rescaling of j_* is contradicted by the good agreement between different estimates of j_* for individual disk-dominated galaxies shown in the middle panels of Figure 4. The only discrepant points here belong to galaxies with significant bulges ($\beta_* > 1/3$), where the different methods of disk–bulge decomposition and assumptions about bulge rotation matter. The rescaling of j_* is another reason Sweet et al. (2018) found a high value of the exponent ($\alpha \approx 1$) in their combined j_* – M_* relation.

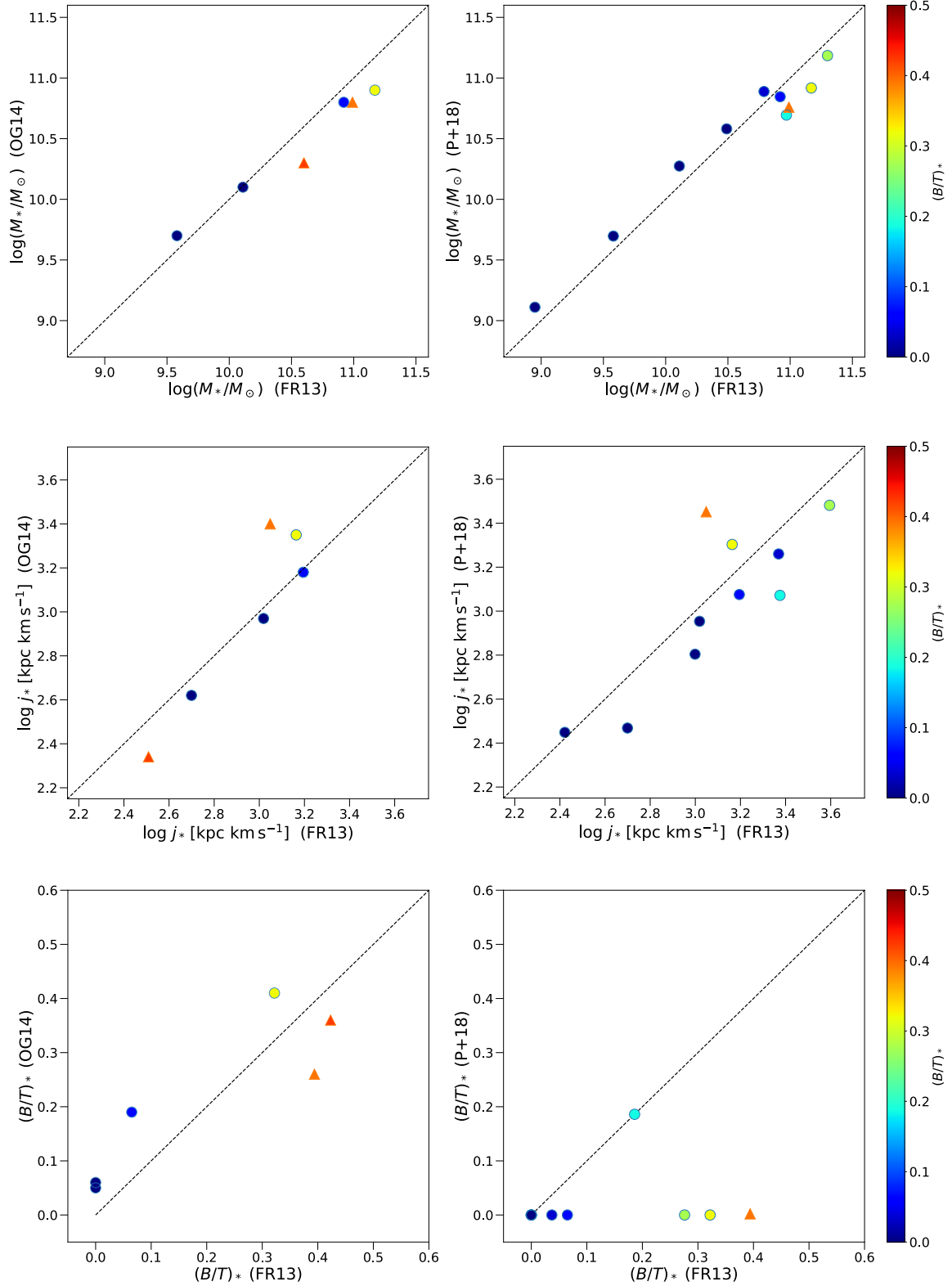


Figure 4. Comparison of stellar specific angular momentum j_* , stellar mass M_* , and stellar bulge fraction, $\beta_* \equiv (B/T)_*$, from our work (Paper 2, FR13), Obreschcow & Glazebrook (2014, OG14), and Posti et al. (2018a, P+18) for the galaxies in common between these samples. The colors and shapes of the plotted symbols indicate the bulge fractions from our dataset, with circles for $0 \leq \beta_* < 1/3$, triangles for $1/3 \leq \beta_* < 2/3$, and squares for $2/3 \leq \beta_* \leq 1$. Note that the color scale here differs from that in Figure 1. The dashed diagonal lines indicate the one-to-one relations. Note that there are no systematic discrepancies between these independent estimates, apart from a tendency by Posti et al. to assign $\beta_* = 0$ to galaxies with small bulges.